



PAPER

Synthesis, characterization and properties of hierarchically assembled antimony oxyhalides nanonetworks

To cite this article: N Komal et al 2019 Mater. Res. Express 6 065035

View the article online for updates and enhancements.

You may also like

- Tunable crystallization mechanism of Sb₂Te films by VO₂ nano-grid framework for breaking through the trade-off between thermal stability and crystallization speed Yang Li and Yegang Lu
- Vertical strain-induced modification of the electrical and spin properties of monolayer MoSi₂X_± (X = N, P, As and Sb)
 Shoeib Babaee Touski and Nayereh Ghobadi
- Molecular dynamics simulation of interaction between nanorod and phospholipid molecules bilayer Xin Wang, , Xiang-Qin Li et al.



Materials Research Express



RECEIVED

20 November 2018

REVISED

3 March 2019

ACCEPTED FOR PUBLICATION

7 March 2019

PUBLISHED

22 March 2019

PAPER

Synthesis, characterization and properties of hierarchically assembled antimony oxyhalides nanonetworks

N Komal¹, Z Malik^{1,2}, N Z Ali^{3,4} and A J Chaudhary²

- Department of Chemistry, School of Natural Sciences, National University of Sciences & Technology (NUST), H-12, Islamabad-44000, Pakistan
- Institute of Environment, Health and Societies, Brunel University London, Uxbridge, UB8 3PH, United Kingdom
- Joint International Centre for Advanced Nanomaterials & Defect Engineering, National Centre for Physics (NPU-NCP), Quaid-I-Azam University, Islamabad-44000, Pakistan
- ⁴ Federal Institute for Materials Research and Testing (BAM), Richard-Willstaetter-Strasse 11, 12489 Berlin, Germany

E-mail: zahida.malik@sns.nust.edu.ple

Keywords: nanorods, nanosheets, antimony oxychloride (Sb₄O₅Cl₂), optical properties, dielectric properties

Abstract

The novel synthesis route has been developed for hierarchically structured; nanorods and nanosheets of Sb₄O₅Cl₂ from a single precursor, with dimension range between 57–90 nm. X-ray powder diffraction analysis confirmed the monoclinic crystal symmetry in $P2_1/c(14)$ with structure type $Sb_4O_5Cl_2$ for both forms; the nanorods and nanosheets. Rietveld refinements and crystallite size investigations of the powder patterns revealed significant enhancement in intensity with subtle variation in the lattice parameters and crystallite size decrease in case of nanosheets in comparison to the nanorods assembly. Through scanning electron microscopy, a composition commensurate to Sb₄O₅Cl₂ at% with averaged dimensions; dia. \sim 90 nm, $l \sim 2 \mu m$ for nanorods and dia. \sim 50–150 nm for nanosheets got corroborated. Owing to the quantum confinement a band gap widening was observed while moving from bulk to nano regime, i.e. 3.25, 3.31 and 3.34 eV, for bulk, nanosheets, and nanorods, respectively. In the case of nanosheets, the highest value of dielectric constant was observed, i.e. 87, as compared to nanorods and the bulk, i.e. 40 and 35.5, respectively. The nanosheets also showed the highest value of dielectric and tangent loss with an increase in frequency due to the least crystallite size of these nanonetworks. Nanosheets depicted the higher AC conductivity at low frequency due to the alignment of the charges but its value decreases at the higher frequency due to lack of time for charge reorientation. The hopping phenomenon was observed in all three cases with the most prominent one in bulk case at higher frequencies.

1. Introduction

Since last few decades, extensive studies on synthesis and properties of nanomaterials prove that the nanostructuring of material in one, two and three dimensions leads to novel optical, electrical and mechanical properties [1, 2]. There are numerous reports on one-dimensional nanomaterials synthesis [3] along with their applications in nanodevices and nanocomposites industries [4]. Antimony-based compounds, e.g. antimony oxide and antimony oxyhalides have great recognition as flame retardants, catalysis, and application in optical devices [5–7]. Particularly, antimony oxychlorides $Sb_4O_5Cl_2$ has applications as a photocatalyst for degradation of dyes and better flame retardants as compare to other Sb-based materials [8, 9]. Due to its multi-faceted applications researchers have been constantly trying to develop various synthetic routes for controlled growth of $Sb_4O_5Cl_2$.

The first report on $Sb_4O_5Cl_2$ crystal structure with monoclinic geometry $(P2_1/c)$ was documented by Edstrand in 1947 [10], followed by Sarnstrand's work [11] documenting the same crystal structure but with different Sb-O distances. Later in 2006, a hydrothermally synthesized $Sb_4O_5Cl_2$ structure was also reported [12].

In near past different antimony oxychlorides are synthesized; Sb_3O_4Cl (new structure P2/c) [13], SbOF, SbOCl [14, 15] and $Sb_8O_{11}X_2$ (X = Cl, Br) [16]. The solid state and wet chemical synthesis routes provide various nanostructures and morphologies with different starting precursors. Recently, the Sb₈O₁₁Cl₂(H₂O)₆ needle-like microstructures with dimensions; dia. = $2 \mu m$ and length $< 20 \mu m$, are prepared by Li et al by employing antimony trichloride, hydrochloric acid, and ethanol as precursor and solvent, respectively [17]. An electrochemical method with Sb anode, different metal cathodes and chloride salt dissolved in HCl also produces Sb₄O₅Cl₂ [18]. The hydrothermal approach with SbCl₃, NaOH and ethylene glycol gives Sb₄O₅Cl₂ and Sb₈O₁₁Cl₂ nanocrystals [19]. Same approach yields antimony oxychloride nanowires by using SbCl₃, ethanol, and NaOH with different dimensions against variable reaction times; nanowire bundles (dia. = 60–110 nm, l=2–5 μ m) and uniformly self-oriented nanowires (dia. = 100–130 nm, $l\sim 1~\mu$ m) for 2 and 20 h, respectively [20]. Sheaf-like antimony oxychloride $[Sb_8O_{11}Cl_2.(H_2O)_6]$ microcrystals (dia. = 270 nm, $l = 3-4 \mu m$) are possible to obtain from SbCl₃, ethylene glycol, PVP (polyvinylpyrrolidone) [5]. An HCl leaching process yields 99.5% antimony oxychloride from high-arsenic refined bismuth dust [21]. Whereas, pH-regulated templatefree method provides Sb₄O₅Cl₂ with different nanostructures from SbCl₃, ethyl alcohol and ammonia [8]. The composites of Sb₄O₅Cl₂ are also reported; PbCl₂/Sb₄O₅Cl₂ [22] (by simple solution method), Sb₂S₃/Sb₄O₅Cl₂ [23] (hydrothermally) and $g-C_3N_4-Sb_2S_3/Sb_4O_5Cl_2$ (hydrothermally) [24]. No doubt these methods give a good yield of halogenated antimony oxides but at least one solvent other than water is a must need for the shape and size control. Moreover, these techniques are tricky and time taking. To the best of our knowledge, this is the 1st study that investigates the synthesis of two different nanostructures of antimony oxychloride prepared via facile method using a sole precursor route. The convenient handling and utilization of a single precursor without the use of any non-aqueous solvents is the key point of the study. We report here simplistic approach for the synthesis/control of one dimensional (ID) nanorods and nanosheets along with the comparison of their optical and dielectric properties with that of the bulk counterpart. A distinctive consideration has paid to the refinement of crystal structure, band gap calculations and dielectric parameters of all prepared materials. Moreover, in this comparative study, a comprehensive overview of dielectric properties of all Sb₄O₅Cl₂ prepared samples is illustrated.

2. Experimental

2.1. Synthesis

The white precipitates were obtained by ultrasonication of 2 mM aqueous solution of antimony (III) trichloride (BDH grade with purity >99%) for 2.5 h at 45 °C. The chemistry of reaction is given below [25],

$$4SbCl_3 + 5H_2O \rightarrow Sb_4O_5Cl_2 + 10HCl$$

Afterward, the precipitate suspension was centrifuged @12 000 rpm for 15 min followed by 2–3 times washing with distilled water. To remove impurities, the washing of precipitates was accomplished by centrifuging @10 000 rpm for 10 min. To study the effect of drying atmosphere over the morphology of prepared sample it was divided into two parts and dried under two distinct conditions; (a) under vacuum at 70 °C for 2 h and (b) ambient condition at 70 °C for overnight. The vacuum drying yielded nanosheets while open-air drying of the sample gave nanorods.

2.2. Characterization

2.2.1. X-ray powder diffraction

X-ray powder diffraction data were collected from powders of as cast and annealed states employing an STOE Germany system with monochromatic $CuK_{\alpha 1}$ radiation ($10^{\circ} < 2\theta > 80^{\circ}$) operated at 40 kV. The Rietveld refinement technique was executed for both the qualitative and quantitative structural refinement with the TOPAS program (version 4.1, Bruker AXS).

2.2.2. Scanning electron microscopy (SEM)

To ascertain sample morphologies, structure hierarchy and qualitative analysis, scanning electron microscopy (SEM) via Electron Probe Micro Analysis (EPMA) on a Zeiss Supra 55 VP equipped with an EDX system operated at 10 kV was employed over the samples coated by standard procedures.

2.3. Physical properties

2.3.1. UV-vis diffuse reflectance spectroscopy

Optical properties were measured by PerkinElmer UV/VIS/NIR spectrometer Lambda 950 with a spectral range of 190–3300 ${\rm cm}^{-1}$ over the powder samples.

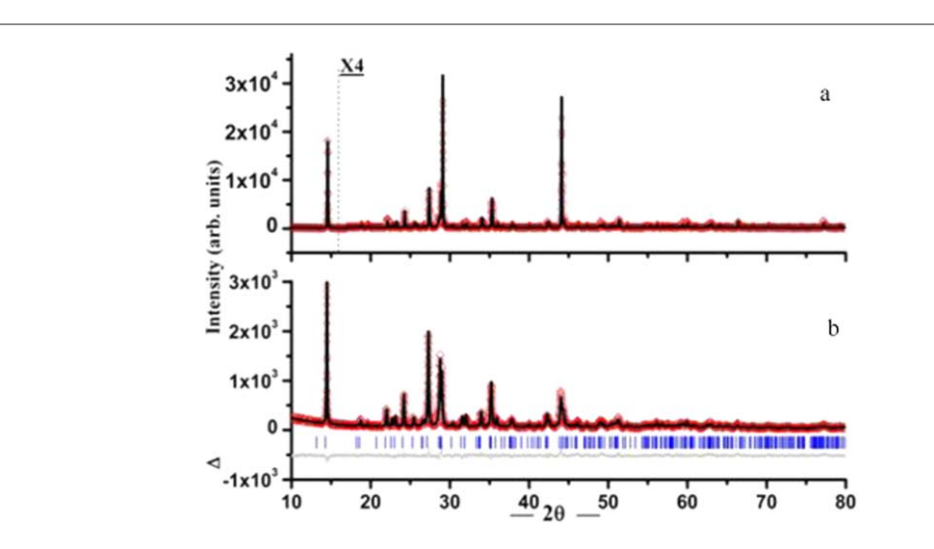


Figure 1. Diffracted x-ray intensities for a polycrystalline samples; (a) nanosheets, (b) nanorods of $Sb_4O_5Cl_2$ at T=298 K as function of diffraction angle 2θ ($\lambda=1.5409$ Å), shows the observed pattern (diamonds), the best Rietveld-fit profile (black line), reflection mark (vertical bars), and difference plot $\Delta=I_{obs}-I_{calc}$ (gray line) (shifted by a constant amount \times 4).

2.3.2. Dielectric properties

The pellets of dia = 12 mm and thickness = 2.3 mm were prepared mechanically by hydraulic press employing 10 MPa pressure for 10 min at room temperature. For dielectric properties, pellets were fixed one by one between the electrodes of Wayne Kerr model 6500B LCR meter having a frequency range of 100 Hz-5 MHz for measurements at room temperature.

3. Results and discussion

3.1. Structural refinement and morphological description

The Rietveld refinement of XRD data confirmed the successful synthesis of single phase antimony oxychloride ($Sb_4O_5Cl_2$) nanorods while minute impurity (<3%) of Sb_2O_4 phase was observed in nanosheets samples. The structural coordinates reported by Edstrand [10] and Särnstrand [11] were taken as starting parameters for structural refinement. The crystallographic structural refinement revealed that all the observed diffraction peaks of both; the nanorods and nanosheets of $Sb_4O_5Cl_2$ were possible to index quite meticulously to monoclinic structure ($P2_1/c$, PDF number: 01-070-1102) as shown in figure 2(a). Moreover, extension in size of $Sb_4O_5Cl_2$ nanorods led to the splitting at the two ends into long slices further extension in length resulted in the transformation of these nanorods into the nano-belt shaped sheet-like structures. This phenomenon was also evident during the Rietveld refinement of texture effect precisely via a preferred orientation function that enabled us to correct the intensities much better as shown in figure 1.

The qualitative Rietveld structural refinement of PXRD data revealed that the unit cell of $Sb_4Cl_2O_5$ contains two assorted Sb atoms positions [(Sb(I) and Sb(II)] with distinct coordination polyhedron around each antimony as further endorsed from the respective distinct bond length of Sb-O. Sb(II) atoms were coordinated via three oxygen atoms in trigonal bipyramids (SbO₄E) geometry with one of the equatorial corners of Sb(II) occupied by electrons lone pair and secondly the Sb(I) atoms were coordinated in tetrahedral geometry (SbO₃E) to oxygen atoms where the lone pair is around one of the four corners of Sb(I). These tetrahedrally coordinated Sb(I) cations were further edge shared via O3 atoms and form dimers, which were connected via vertices to neighboring dimers by O1 atoms ultimately forming zig-zag tetrahedral chains within each two dimensional $(Sb_4O_5^{2+})_n$ puckered layers. The coordination polyhedra of Sb(I) and Sb(II) were observed to further linked via oxygen atoms forming an infinite two-dimensional network of $(Sb_4O_5^{2+})_n$ layers outspreading parallel to bcplane. Owing to the lone pair effect of Sb, both Sb(I) and Sb(II) atoms were directed outwards from the layers with Cl $^-$ ions sandwiched in between the $(Sb_4O_5^{2+})_n$ layers as shown in figure 2(b). A remarkable increase in intensities at certain Bragg reflections over the others in the XRD patterns were observed. To better assess the background fit, the intensity data around the y-axis were plotted in square root scale which further helped in reducing the reliability/residual factor to a lower R-values, selected lattice parameters along with and R-values are reported in table 1.

The qualitative analysis and morphologies of the samples were determined by SEM. The SEM micrograph of the nanosheets and nanorods of antimony oxychloride are shown in figures 3 and 4. There was an observation of two different nanostructured morphologies by varying the drying condition. According to nucleation theory

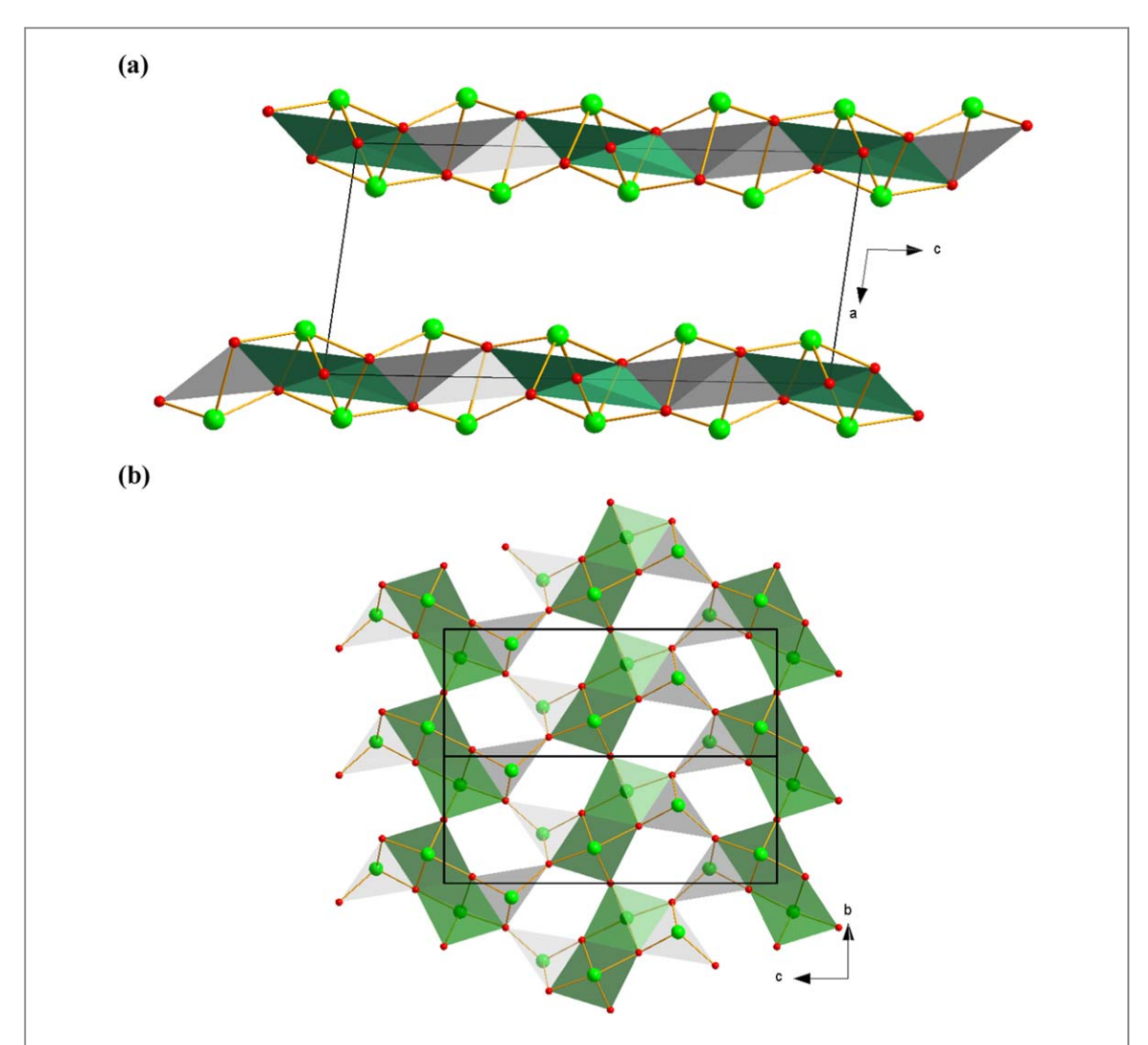


Figure 2. The [Sb₄O₅²⁺] layers of linked coordination polyhedra, (a) packing model along the b-direction and, (b) along the bc plane of the monoclinic crystal structure (2 \times 1 \times 2 supercell) of Sb₄O₅Cl₂. The figure depicts Sb(1), coordinated to four oxygen atoms (Green polyhedra) while Sb(2), considered to be three coordinated (Grey triangles). The oxygen atoms and antimony atoms are shown in red and green colors, respectively (The Cl atoms are omitted for clarity).

Table 1. The crystal structure and lattice parameters extracted via Rietveld refinements for $\mathrm{Sb_4O_5Cl_2}$ nanostructures, crystallized in space group: $P2_1/c$ #14.

Parameters	Nanorods	Nanosheets
a(Å)	6.2029(7)	6.241 97(15)
b(Å)	5.0854(8)	5.113 90(33)
c(Å)	13.473(2)	13.542 97(98)
β(°)	97.194(8)	97.2403(34)
$d(g \text{ Cm}^{-3})$	5.0249(12)	4.941 18
$Vol(Å^3)$	421.63(10)	428.856(43)
R_{bragg}	7.371	12.174
R _{exp}	8.321	7.667
GOF	2.129	3.449

[26],

$$N = A \exp(-\Delta G^*/RT)$$

Where N is Nucleation density, A is a proportionality constant and ΔG^* is the activation energy for nucleation. ΔG^* has two components, ΔG_s (Surface free energy) and ΔG_v (volume free energy). Moreover, $\Delta G_v \propto -ln$ (O_2), according to this relation the activation energy of nucleation is very high and nucleation density is low in case of vacuum, i.e, low concentration of oxygen. So in the vacuum it resulted in the synthesis of nanosheets with

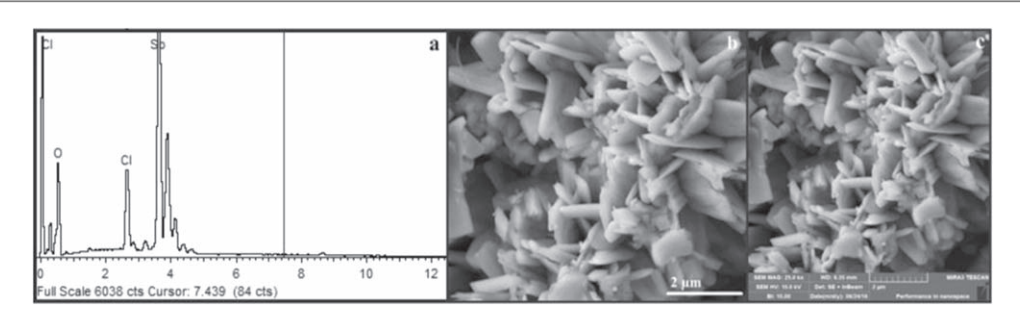


Figure 3. SEM micrographs of $Sb_4O_5Cl_2$ nanosheets with EDX spectrum, 3(a) and (b) show $Sb_{33.73}O_{50.73}Cl_{15.54}$ at% composition and overall morphology, 3(c) shows one dimension of nanosheets which lies in a range of 50–150 nm.

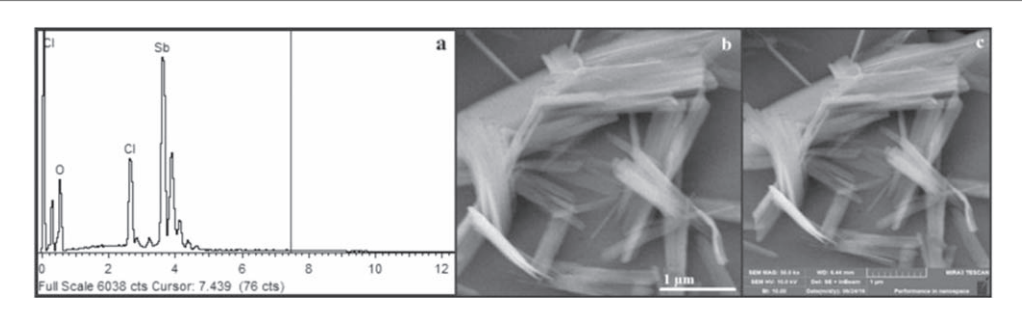


Figure 4. SEM micrographs of Sb₄O₅Cl₂ nanorods with EDX spectrum, 4(a) and (b) show Sb_{33,28}O_{52,28}Cl_{12,5} at% composition and overall morphology, 3(c) shows 1D nanorods with dimensions; $l \sim 2 \mu m$ and dia. = 90 nm.

small crystallite size, i.e. 57.7 nm. Whereas in open air drying nanorods were obtained due to higher oxygen content, the overall ΔG^* was low and the nucleation density was high. This fact was verified by crystallite size of nanorods, i.e. 90 nm. The average crystallites sizes were calculated by Debye- Scherrer formula [27].

In figures 3(a) and (b) images present composition and overall morphology while figure 3(c) shows one dimension of nanosheets which lies in a range of 50–150 nm and Sb_{33.73}O_{50.73}Cl_{15.54} at% composition. Similarly, figures 4(a) and (b) show composition and overall morphology of antimony oxychloride nanorods while 1D nanorods are confirmed by figure 4(c) with the composition, Sb_{33.28}O_{52.28}Cl_{12.5} at%. The synthesized nanorods have $l \sim 2~\mu \text{m}$ and dia. = 90 nm. The extra peaks in EDX spectra can be attributed to sample holder and graphite coating material.

3.2. Physical properties

3.2.1. Optical properties

UV-vis absorption spectroscopy was not much useful for the optical properties of antimony oxychloride nanomaterials. Despite the particle size reduction up to $<100\,$ nm it was still difficult to get an ideal suspension of antimony oxychloride in available solvents. Whereas, UV-vis DRS (Diffused Reflectance Spectroscopy) was a better technique for the band gap evaluation in such case. In reflectance spectra provided in figure 5(a), the maximum reflectance was obvious at about 405 nm. The figure 5(a) shows that as we move from bulk to nano regime the % reflectance enhances about 55 to 100% due to presences of a greater number of surface atoms that have the ability to reflect the incident radiations. Moreover, a slight shift of reflectance toward higher wavelength was due to enhanced oscillator strength at higher wavelength and dominance of surface plasmon resonance. The calculated band gap values (3.34–3.25 eV) matched well with the reported ones. According to literature, the electronic band gap of Sb₄O₅Cl₂ lies in the range of 3.25–3.38 eV [9]. A well-explained trend of a blue shift in band gap with decreasing particle size was observed. As we move from bulk to nanorods, the electronic band gap value was increased due to the quantization effect. These studies also revealed that change of technique from UV-vis absorption spectroscopy to UV-vis DRS does not have any effect on the electronic band gap of Sb₄O₅Cl₂.

Further, this study revealed that nanostructures of antimony oxychloride have better reflectance ability as compared to its bulk counterpart. The DRS study also allowed the calculation of band gap through Tauc's plot (a plot of energy (eV) versus $(hv\alpha)^n$) [28] by replacing the absorption factor with reflectance factor F(R) employing Kubelk-Munk expression given below [29],

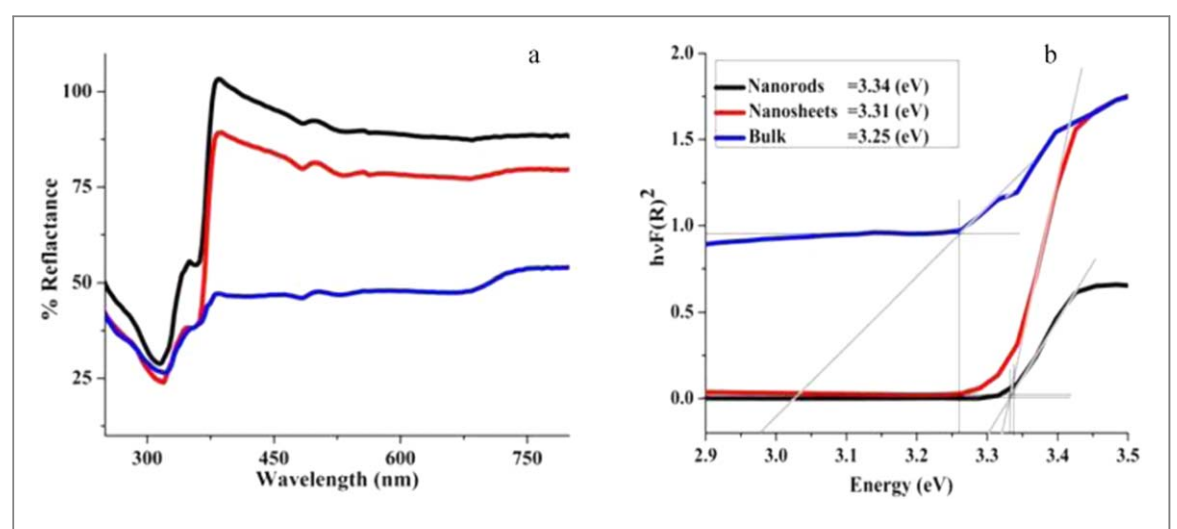


Figure 5. Optical properties, (a) wavelength verses % reflection of $Sb_4O_5Cl_2$ bulk, nanorods and nanosheets, (b) band gap values of $Sb_4O_5Cl_2$ bulk, nanorods, and nanosheets.

$$F(R) = \frac{(1-R)^2}{2R} = \frac{K}{S}$$

Where R is absolute reflectance, K is molar absorption coefficient and S is a scattering coefficient. A plot of Energy (eV) versus $hvF(R)^2$ was plotted to approximate the value of E_g . In figure 5(b), the graph shows the estimated values of the band gap for nanorods, nanosheets, and bulk, i.e. 3.34, 3.31 and 3.25 eV, respectively. These results disclosed that as we move from bulk to nano-antimony oxychloride, the band gap increases from 3.25 to 3.34 eV.

3.2.2. Dielectric properties

Dielectric properties are comprised of four main components; (i) dielectric constant, (ii) dielectric loss, (iii) tangent loss and (iv) AC conductivity, which are the important parameters to explore the device application of materials. We explain all these components one by one in the following paragraphs for nanosheets, nanorods and bulk materials. Dielectric constant (ε) provides information about the ability of the material to become polarize (polarizability of material) or capacity of the material to store applied electric energy. The value of dielectric was calculated by using the following expression,

$$\varepsilon = \frac{C \times d}{\varepsilon_o \times A}$$

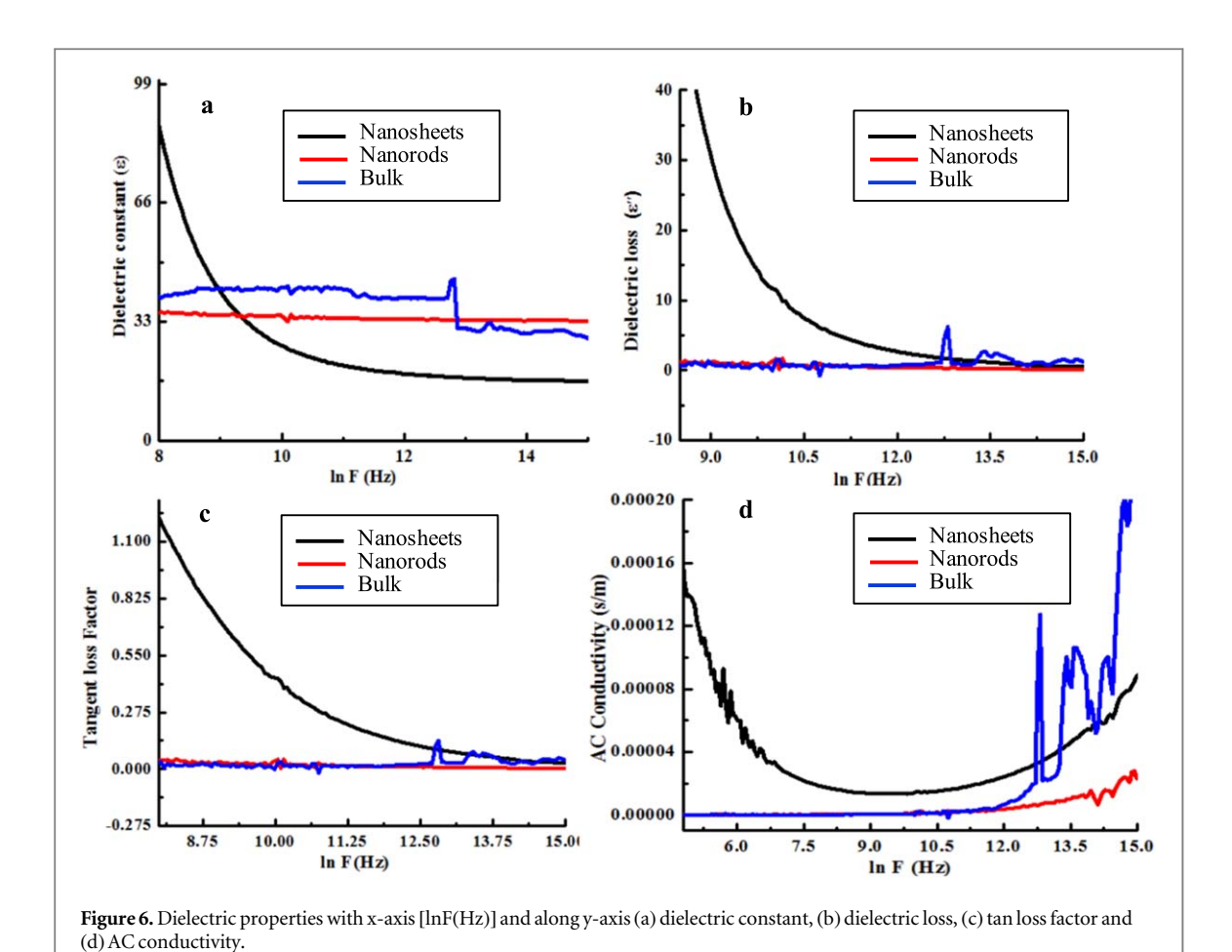
Where C is capacitance, d is the sample thickness, ε_0 is permittivity of free space having value $8.85 \times 10^{-12} \, \mathrm{Fm^{-1}}$ and A is the surface area of a sample [30]. Dielectric loss (ε'') or dissipation factor is an imaginary part to determine the loss of electromagnetic energy or the electromagnetic energy that is dissipated to align the particles along the applied electric field. The real part to calculate the energy loss is called tangent loss ($\tan \delta$) while dissipation factor quantitatively parameterized by using the term known as tangent loss factor. The equations for these two factors are given below [30, 31],

$$\varepsilon'' = \varepsilon \times Dfactor$$
$$\tan \delta = \frac{\varepsilon''}{\varepsilon}$$

Lastly, AC conductivity (σ_{ac}) is the capacity or ability of the material to allow the passage of an alternating current which can be calculated σ_{ac} by the below-given formula,

$$\sigma_{ac} = 2\pi f \varepsilon_o \varepsilon'' \tan \delta$$

Out of four types of polarization, i.e., electronic, ionic/atomic, dipolar or orientational and interfacial polarization, we usually come in contact with dipolar or orientational polarization which takes place at a frequency about 1 kHz–1 MHz. The plot of $\ln(F)$ and ε (given in figure 6(a)) shows a higher value of ε for nanosheets (~87) as compared to nanorods (~40) and bulk (~35.5). Nanosheets of antimony oxychloride showed an ideal response toward the applied electric field and the decrease in value of dielectric constant was observed with increase in frequency because at a higher frequency the particles lack in time to orient themselves according to the applied field. Therefore, the passage of electron becomes possible at a higher frequency. While in the case of nanorods and bulk form of antimony oxychloride, there was no significant effect of frequency so the value of dielectric constant almost remained the same for the whole frequency range. The dielectric constant



mainly gets affected by microstructure, crystallite size and no. of grain boundaries encounter. An inverse relationship has been observed between dielectric constant and the crystallite or grain size of material [32]. Whereas, dielectric properties are independent of the geometry or dimensions of material along any axis. As the crystallite size increases the value of dielectric constant decreases because less separating boundaries encounter and particles can align themselves at low frequency [33]. The calculated values of average crystallite size via Debey-Scherrer formula [27] for nanosheets, nanorods and bulk form of antimony oxychloride were 57.7 nm, 90.2 nm and 104.2 nm, respectively. These values depicted an enhancement in dielectric constant for nanosheets due to presences of the greater number of separating boundaries that come across and resist the alignment of particles at the lower frequency. This variation in crystallite size led to the decreased value of dielectric constant as we moved from nanosheets towards nanorods and bulk form. A similar trend for dielectric loss and tangent loss observed for nanosheets, nanorods, and bulk antimony oxychloride as provided in figures 6(b) and (c). The measured values of dielectric loss for nanosheets, nanorods, and bulk were 40, 1.4 and 0.5, respectively. The tan loss is 1.2 in case of nanosheets and approximately near to zero for nanorods and bulk antimony oxychloride. Another important component to determine dielectric behavior is AC conductivity, graph between ln(F) and AC conductivity is shown in figure 6(d) which depicts that nanosheets have higher value of AC conductivity at lower frequency (5 kHz), because the particles can easily align themselves to applied field and permits the flow of electrons. But at some higher frequency (7 kHz), the particles had not enough time to orient themselves according to the applied field. At this frequency, AC conductivity got a decrease due to the arbitrary motion of particles in all directions and caused resistance in the passage of current. Nanorods and bulk did not have such a prominent response toward AC conductivity due to some structural imperfections. At highest frequencies (12 kHz), a phenomenon of hopping was observed in all three cases with the most prominent one in bulk case. When the frequency of electron transfers from one atom to another atom became equal to the applied frequency, resonance took place. This resonance caused the enhancement in amplitude that was observed in form of hop in the graph, may be due to some defects in the structure.

4. Conclusions

It is concluded that two different nanoforms of single phase Sb₄O₅Cl₂ have been prepared successfully by employing a single source precursor via wet chemical strategy. The detailed crystal structure, crystallite size, morphology, geometry, and composition of materials have been investigated by employing XRPD, EDX and the SEM analysis. Afterward, optical and dielectric properties along with a comparison with the bulk counterpart have been investigated thoroughly. These observations depict that Sb₄O₅Cl₂ is a semiconductor whose band gap increases as we move from bulk to the nano regime. While dielectric studies show that nanosheets have the highest value of dielectric constant, dielectric and tangent loss with the increase in frequency due to the least crystallite size of the material. These properties; semiconducting nature, smaller crystallite and particle size make these materials the potential candidates in energy storage devices and as the potent flame retardants.

Acknowledgments

We highly acknowledge the facilities and technical support provided by Institut für Mineralogie und Kristallographie, University of Vienna, Althanstraße 14 1090 Vienna, Austria, School of Chemical Material Engineering (SCME) and School of Mechanical & Manufacturing Engineering (SMME), NUST, Islamabad, Pakistan. We also acknowledge the HEJ Research Institute of Chemistry, University of Karachi, Karachi-75270, Pakistan.

Conflict of Interest

The authors declare that they have no conflict of interest.

References

- [1] Mazzoni M S C, Choi H J, Ihm J, Louie S G, Zettl A and McEuen P L 2000 Science 288 494-97
- [2] Ohtsuka S, Koyama T, Tsunetomo K, Nagata H and Tonaka S 1992 Appl. Phys. Lett. 61 2953
- [3] Han W Q, Fan S S, Li Q Q and Hu Y-D 1997 Science 277 1287
- [4] Guo L, Wu Z, Liu T, Wang W and Zhu H 2000 Chem. Phys. Lett. 318 49
- [5] Zhou J, Zhao H, Li L, Tian M, Han J, Zhang L and Guo L 2011 J. Nanosci. Nanotechnology. 11 8504-09
- [6] Wang Y and Lee J Y 2006 Angew. Chem. Int. Ed. 45 7039
- [7] Matsuzawa K, Shido T and Iwasawa Y 2003 Langmuir 19 2756
- [8] Costa L, Goberti P, Paganetto G, Camino G and Sgarzi P 1990 Polym. Degrad. Stab. 30 13
- [9] Yang L, Huang J, Cao L, Shi L, Yu Q, Kong X and Jie Y 2016 Sci. Rep. 6 27765
- [10] Edstrand M 1947 Acta Chem. Scand. 1 178
- [11] Sarnstrand C 1978 Acta Crystallographica Section B: Structural Crystallography and Crystal Chemistry 34 2402
- [12] Su X, Liu Y, Xiao C, Zhang G, Liu T, Qin J and Chen C 2006 Mater. Lett. 60 3879
- [13] Katzke H, Oka Y, Kanke Y, Kato K and Yao T 1999 Z. Kristallogr. 214 284
- [14] Åström A 1972 Acta Chem, Scand, 26 3849
- [15] Åstrom A, Andersson S and Sol J 1973 State Chem. 6 191
- [16] Mayeroyá Z. Johnsson M and Lidin S 2006 Solid State Sci. 8 849
- [17] Li B, Zhao Y, Xu X, Zhou H, He B, Wu Z S and Zhang Z J 2007 Ultraso. Sonochem. 14 557
- [18] Bo Z, Meihua M and Jiansheng G 2007 Chinese Journal of Applied Chemistry 24 226
- [19] Chen XY, Huh HS and Lee SW 2008 J. Solid State Chem. 181 2127
- [20] Tang J J, Wang Y, Jiao Z and Wu M 2009 Mater. Lett. 63 1481
- [21] Zheng Y J, Teng H and Bai M 2011 Journal of Central South University (Science and Technology) 42 1549
- [22] Li P, Shu J, Shao L, Lin X, Wu K, Shui M, Wang D, Long N and Ren Y 2014 J. Electroanal. Chem. 731 128
- [23] Jiang Q, Yuan X, Wang H, Chen X, Gu S, Liu Y, Wuab Z and Zengab G 2015 RSC Adv. 5 53019
- [24] Liu Y, Yuan X, Wang H, Chen X, Gu S, Jiang Q, Wu Z, Jiang L, Wu Y and Zeng G 2015 Catalytic Communication 70 17
- [25] Li C, Yang X, Liu Y, Zhao Z and Qian Y 2003 J. Cryst. Growth 255 342
- [26] Ohring M 1992 The Materials Science of Thin Films 1 (London: Academic)
- [27] Azároff L V and Buerger M J 1958 The Powder Method in X-ray Crystallography 3 (New York: McGraw Hill)
- [28] Chandran A, Francis N, Jose T and George K C 2010 Academic Review XVII 17
- [29] Ganguly M, Rout S K, Park H Y, Ahn C W and Kim I W 2013 Physics Express 3 1
- - Hermann A M and Yakhmi J V 1994 Handbook of Superconducting Materials (New York: Dekker)
- [31] Kayed T S 2003 Mater. Res. Bull. 38 533
- [32] Kinoshita K and Yamaji A 1976 J. Appl. Phys. 47 371

[30] Sheng Z Z and Hermann A M 1988 Nature 55 332

[33] Chintaparty R and Reddy N R 2016 Adv. Mater. Lett. 7 235